Phosphorescent Binuclear Iridium Complexes Based on Terpyridine−Carboxylate: An Experimental and Theoretical Study

ARTICLE *in* INORGANIC CHEMISTRY · AUGUST 2011

Impact Factor: 4.76 · DOI: 10.1021/ic200704s · Source: PubMed

8 AUTHORS, INCLUDING:

Eugen S. Andreiadis
Atomic Energy and Alternative Energies Com…
18 PUBLICATIONS **401** CITATIONS
SEE PROFILE

Daniel Imbert
Atomic Energy and Alternative Energies Com…
72 PUBLICATIONS **2,399** CITATIONS
SEE PROFILE

Adrian Calborean
National Institute for Research and Develop…
25 PUBLICATIONS **147** CITATIONS
SEE PROFILE

Marinella Mazzanti
École Polytechnique Fédérale de Lausanne
147 PUBLICATIONS **3,545** CITATIONS
SEE PROFILE

Inorganic Chemistry

ARTICLE

pubs.acs.org/IC

Phosphorescent Binuclear Iridium Complexes Based on Terpyridine−Carboxylate: An Experimental and Theoretical Study

Eugen S. Andreiadis,[†] Daniel Imbert,[†] Jacques Pécaut,[†] Adrian Calborean,[*,‡] Ilaria Ciofini,[‡] Carlo Adamo,[‡] Renaud Demadrille,[§] and Marinella Mazzanti[*,†]

[†]Laboratoire de Reconnaissance Ionique et Chimie de Coordination, SCIB, UMR-E 3 CEA/UJF-Grenoble 1, INAC, Grenoble, F-38054, France

[‡]Laboratoire d'Electrochimie, Chimie des Interfaces et Modélisation pour l'Energie (UMR CNRS 7575), Ecole Nationale Supérieure de Chimie de Paris, Chimie-ParisTech, 75231 Paris, France

[§]Laboratoire d'Electronique Moléculaire Organique et Hybride, UMR5819-SPrAM, CEA-CNRS-University Grenoble I, INAC, CEA-Grenoble, 38054 Grenoble, France

Supporting Information

ABSTRACT: The phosphorescent binuclear iridium(III) complexes tetrakis(2-phenylpyridine)μ-(2,2′:6′,2″-terpyridine-6,6″-dicarboxylic acid)diiridium (**Ir1**) and tetrakis(2-(2,4-difluorophenyl) pyridine))μ-(2,2′:6′,2″-terpyridine-6,6″-dicarboxylic acid)diiridium (**Ir2**) were synthesized in a straightforward manner and characterized using X-ray diffraction, NMR, UV−vis absorption, and emission spectroscopy. The complexes have similar solution structures in which the two iridium centers are equivalent. This is further confirmed by the solid state structure of **Ir2**. The newly reported complexes display intense luminescence in dichloromethane solutions with maxima at 538 (**Ir1**) and 477 nm (**Ir2**) at 298 K (496 and 468 nm at 77 K, respectively) and emission quantum yields reaching ∼18% for **Ir1**. The emission quantum yield for **Ir1** is among the highest values reported for dinuclear iridium complexes. It shows only a 11% decrease with respect to the emission quantum yield reported for its mononuclear analogue, while the molar extinction coefficient is roughly doubled. This suggests that such architectures are of potential interest for the development of polymetallic assemblies showing improved optical properties. DFT and time-dependent-DFT calculations were performed on the ground and excited states of the complexes to provide insights into their structural, electronic, and photophysical properties.

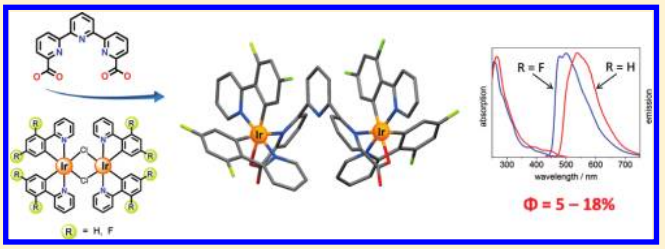

INTRODUCTION

In recent years, iridium(III) complexes and, in particular, cyclometalated complexes with phenylpyridine-based ligands have emerged as attractive materials especially for the development of organic light-emitting diodes (OLED) for displays and low-energy lighting devices[1−7] but also for applications as biological labeling agents and phosphorescent sensors.[8−14] This is due to the interesting luminescent properties[15] that they exhibit, such as high emission quantum yields, photo- and thermal stability, long excited-state lifetimes, and easy tuning of the emission color through control of the ligand structure.

An increasingly high number of novel mononuclear cyclometalated Ir(III) complexes has been prepared in the past decade with the objective of optimizing the phosphorescence efficiency and tuning the emission color in Ir-based phosphorescent emitters.[1,7,15−18] Heteroleptic iridium complexes are particularly advantageous because they can be prepared in softer conditions compared to the homoleptic analogues.[19−22] Iridium(III) complexes with very high phosphorescence efficiency in solution and the solid state have been designed and in turn tested as emissive layers in optoelectronic devices exhibiting very good efficiency.[2,16,23,24] However, isomerization and concentration-dependent self-quenching effects can significantly reduce the device performance.[25]

The incorporation of iridium in rigid supramolecular architectures can prevent such deleterious effects and provide essential building blocks in more sophisticated supramolecular materials and devices for advanced applications in organic optoelectronics, biomedical labeling, and light-energy conversion.[26−29] The design of supramolecular architectures containing binuclear iridium(III) complexes linked by a conjugated organic bridge attracts considerable interest also for the investigation of photoinduced electron and energy transfers,[30,31] as the bimetallic systems can exhibit an excited state substantially different from that of simple mononuclear systems.

However, to date, binuclear complexes containing cyclometalated Ir(III) centers bridged by organic ligands remain scarce,[15,25,32−40] despite the interest associated with mononuclear iridium complexes. This is probably due to the synthetic difficulties involved, as evidenced by earlier examples[36,37] for which small yields or mixtures of isomers

Received: April 6, 2011
Published: August 10, 2011

Scheme 1. Synthesis of the Bis-Iridium Complexes Ir1 and Ir2

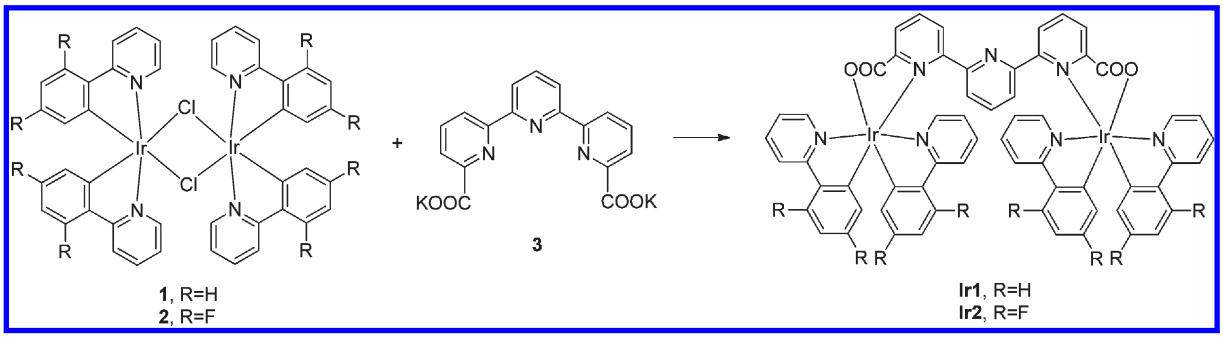

[a]Reaction conditions and yields: ethoxyethanol, 60 °C (86% for **Ir1**, 25% for **Ir2**)

were reported. More successful synthetic approaches, involving cross-coupling of individual iridium units, can be used in the preparation of nonsymmetric systems but require complicated procedures and purification steps.[32,35,38−40] The use of simple bridging ligands is an alternative convenient route for the synthesis of symmetric dinuclear complexes, although the use of neutral bridging units resulted in very modest reaction yields.[33,36]

The quantum efficiencies of the reported dinuclear compounds remain rather low for practical applications (usually below 1%), and few studies have been devoted to the elucidation of the parameters relating structure and photophysical properties. Therefore, it is important to identify new bridging ligands allowing the facile synthesis of rigid binuclear structures with restricted intramolecular motion, capable of preventing isomerization and which can be easily tuned by substitution to modulate the energy of the emissive excited state.

Here, we report the use of the versatile dianionic terpyridine dicarboxylate ligand[41,42] to bridge two phenylpyridine-based Ir(III) complexes in the direct synthesis of two new neutral homobimetallic heteroleptic complexes of iridium. The choice of terpyridine carboxylate acid as an ancillary ligand in iridium(III) complexes was inspired by the good photophysical properties of the mononuclear picolinate-based heteroleptic complexes such as FIrpic (iridium(III) bis[2-(4′,6′-difluorophenyl)pyridinato-N, $C^{2\prime}$]-picolinate).[16,43]

The synthesis, structure, and photophysical investigation of the two new dinuclear iridium complexes tetrakis(2-phenylpyridine)μ-(2,2′:6′,2″-terpyridine-6,6″-dicarboxylic acid)diiridium (**Ir1**) and tetrakis(2-(2,4-difluorophenyl) pyridine) μ-(2,2′:6′,2″-terpyridine-6,6″-dicarboxylic acid)diiridium (**Ir2**) are described and compared with the results obtained using ab initio approaches. In particular, density functional theory (DFT) and time-dependent-DFT (TD-DFT) were applied to model the structural and electronic properties of these systems at the ground and excited states. The nature of the vertical excited state and of the emissive phosphorescent state was analyzed to gain insight into the photophysical properties of such binuclear systems.

RESULTS AND DISCUSSION

Synthesis and Characterization. Our strategy for the formation of neutral bis-iridium complexes bridged by a polyimine ligand is straightforward. The use of a dianionic bridging ligand provides a convenient route for the synthesis of heteroleptic dinuclear iridium complexes. A similar strategy had previously been successfully applied to the synthesis of cationic and neutral mononuclear heteroleptic Ir(III) complexes.[17,44] Reaction of the cyclometalated Ir(III) μ-chloride-bridged dimer $[Ir(ppy)_2\mu Cl]_2$ **1**[17,45] with the potassium salt of terpyridine dicarboxylate **3** in ethoxyethanol at 60 °C leads to the high-yield formation of the desired bis-iridium complex **Ir1** (Scheme 1) as a microcrystalline precipitate, which was easily separated and purified by recrystallization. The reaction proceeds at low temperature because of the dianionic nature of the bridging ligand, preventing the ligand scrambling often observed in the high-temperature synthesis of iridium compounds. Using a similar procedure, the difluorophenylpyridine μ-chloride-bridged precursor $[Ir(F_2ppy)_2\mu Cl]_2$, **2**,[17] was reacted with **3** to afford the bis-iridium complex **Ir2**. The latter was separated and purified by column chromatography, due to its higher solubility in the reaction solvent, compared to the nonfluorinated analogue. The iridium complexes **Ir1** and **Ir2** were fully characterized by ^{1}H NMR spectroscopy, mass spectrometry, and elemental analysis. The fluorinated complexes **2** and **Ir2** were also characterized by X-ray diffraction. Preliminary attempts of stepwise reactivity to prepare nonsymmetric dinuclear complexes from $[Ir(F_2ppy)_2\mu Cl]_2$ and $[Ir(ppy)_2\mu Cl]_2$ lead to a statistical mixture of products, requiring extensive chromatographic purification and compromising the simplicity of the strategy presented. Future work will be directed to explore the possibility of preparing nonsymmetric complexes from different starting compounds.

Molecular and Crystal Structure. The crystal structures of the previously reported iridium precursor **2**[17] and of the new bis-iridium complex **Ir2** were determined by X-ray diffraction studies. Crystals of **2** and **Ir2** suitable for X-ray analysis were obtained by slow evaporation of their chloroform and dichloromethane solutions, respectively. Selected distances and angles between Ir metal and coordinating atoms are given in Table 1, while the full crystallographic data and refinement parameters are available in Table 2.

In the structure of the precursor complex **2**, solved in the $P2(1)/c$ space group of the monoclinic system, each iridium atom is hexacoordinated in a distorted octahedral mode by two cyclometalating difluorophenylpyridine ligands (via the C and N atoms) and two chlorine atoms, which bridge the two iridium centers (Figure 1). The intermetallic distance is 3.77 Å, and the mean values of the Ir−C (1.989(6) Å), Ir−N (2.053(3) Å), and Ir−Cl (2.513(12) Å) bond distances are within the normal ranges expected for such cyclometalated complexes.[44,46] The C−Ir−N bite angles are on average 80.7(3)°, similar to the Cl1−Ir−Cl2 bite angles of 82.6(1)°. The planes of two

dx.doi.org/10.1021/ic200704s |*Inorg. Chem.* 2011, 50, 8197–8206

Table 1. Selected Bond Distances (Å) and Angles (deg) for the Iridium Complexes 2 and Ir2

complex **2**				complex **Ir2**			
Ir1−C1	1.995(7)	C1−Ir1−N1	80.8(3)	Ir1−O1	2.132(6)	O1−Ir1−N1	77.6(3)
Ir2−C23	1.994(7)	C23−Ir2−N3	80.9(3)	Ir2−O3	2.139(6)	O3−Ir2−N3	77.4(2)
Ir1−C12	1.985(6)	C12−Ir1−N2	80.8(3)	Ir1−N1	2.216(7)	N11−Ir1−C31	80.4(3)
Ir2−C34	1.982(7)	C34−Ir2−N4	80.3(3)	Ir2−N3	2.205(7)	N13−Ir2−C71	79.8(3)
Ir1−N1	2.057(5)	Cl1−Ir1−Cl2	82.7(5)	Ir1−N11	2.043(6)	N12−Ir1−C51	80.0(3)
Ir2−N3	2.050(6)	Cl1−Ir2−Cl2	82.6(5)	Ir2−N13	2.050(7)	N14−Ir2−C91	80.8(3)
Ir1−N2	2.054(5)	N1−Ir1−N2	169.7(2)	Ir1−N12	2.036(6)	O1−Ir1−C31	175.2(3)
Ir2−N4	2.051(6)	N3−Ir2−N4	170.5(2)	Ir2−N14	2.039(7)	O3−Ir2−C71	174.8(3)
Ir1−Cl1	2.515(2)	C1−Ir1−Cl1	175.8(2)	Ir1−C31	1.997(8)	N1−Ir1−C51	171.6(3)
Ir2−Cl1	2.500(2)	C23−Ir2−Cl1	172.0(2)	Ir2−C71	1.983(8)	N3−Ir2−C91	172.9(3)
Ir1−Cl2	2.509(2)	C12−Ir1−Cl2	171.9(2)	Ir1−C51	1.997(8)	N11−Ir1−N12	175.9(3)
Ir2−Cl2	2.529(2)	C34−Ir2−Cl2	174.2(2)	Ir2−C91	2.002(8)	N13−Ir2−N14	176.7(3)
		Ir1−Cl1−Ir2	97.4(6)			N1−C6−C7-N2	61.6
		Ir1−Cl2−Ir2	96.8(6)			N2−C11−C12-N3	60.5

Table 2. Crystallographic Data and Refinement Parameters for the Iridium Complexes 2 and Ir2[a]

complex	**2**·3CHCl$_3$	**Ir2**·3CH$_2$Cl$_2$
formula	$C_{47}H_{27}Cl_{11}F_8Ir_2N_4$	$C_{64}H_{39}Cl_6F_8Ir_2N_7O_4$
fw/g·mol^{-1}	1574.08	1719.12
cryst syst	monoclinic	triclinic
space group	*P*2(1)/*c*	*P*-1
a/Å	12.4833(17)	11.905(4)
b/Å	19.596(3)	15.340(5)
c/Å	21.318(3)	18.726(6)
α/deg	90	68.398(6)
β/deg	97.740(3)	73.201(6)
γ/deg	90	76.991(6)
V/Å^3	5167.5(12)	3016.7(16)
Z	4	2
ρ/g·cm^3	2.023	1.893
μ/mm^{-1}	5.783	4.754
θ/°	1.93−26.42	1.44−24.74
reflns collected	19 565	15 265
indep reflns	9340	10 075
parameters	649	948
GOF on F^2	1.010	1.066
R1, wR2	0.0402, 0.0817	0. 0443, 0. 0906
R1, wR2 (all data)	0.0659, 0.0889	0. 0634, 0. 0987

[a] Data in common: λ = 0.71073 Å; T = 223(2) K; refinement method, full-matrix least-squares on F^2; absorption correction, semiempirical from equivalents. wR2 = $[\Sigma[w(F_0^2 - F_c^2)^2]/\Sigma w(F_0^2)^2]^{1/2}$, where $w^{-1} = [\Sigma(F_0^2) + (aP)^2 + bP]$ and $P = [\max(F_0^2, 0) + 2F_c^2]/3$.

cyclometalating ligands and the plane defined by the Cl1−Ir−Cl2 atoms are orthogonal with respect to each other. The coordinating nitrogen atoms are in a trans arrangement, as found typically in the crystal structure of cyclometalated iridium complexes.[37,47,48] This is consistent with the NMR studies of iridium dichloro-bridged dimer complexes reported in the literature, suggesting the presence of species showing the "trans" arrangement of nitrogens,[20,44,49] although recently a mutually cis disposition has been evidenced by NMR studies

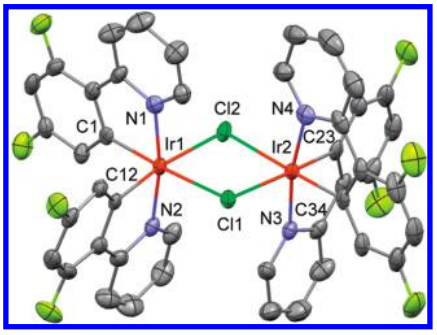

Figure 1. ORTEP drawing of the molecular structure of the iridium complex **2** (thermal ellipsoids at 35% probability level; H atoms omitted for simplicity).

for a iridium dimer containing sulfonyl substituents.[50] In principle, three configurations for the N-trans arrangement can be expected: the achiral meso form ΔΛ in which the two iridium centers are symmetric with respect to one another and the two ΔΔ, ΛΛ enantiomers.[37,49] Crystal structures of the achiral meso form ΔΛ of dinuclear complexes have been previously reported.[37,48] The structure of **2** contains the two ΔΔ, ΛΛ enantiomers, yielding a racemate; the presence of interligand steric interactions probably disfavors the meso form in this complex.

In the structure of **Ir2**, solved in the *P*-1 space group of the triclinic system, each iridium atom is hexacoordinated by the carbon and nitrogen atoms of two cyclometalating difluorophenylpyridine ligands and the nitrogen and oxygen atoms of the terminal picolinate moiety of the terpyridine carboxylate ligand, as shown in Figure 2. The two iridium centers have a distorted octahedral coordination geometry, retaining the *cis*-C,C *trans*-N, N chelate disposition of the chloride-bridged precursor **2.** The structure of the complex contains both the ΔΔ and the ΛΛ enantiomers of the racemic pair. The Ir−C bond distances (on average 1.995(8) Å) are slightly shorter than the Ir−N bond distances (on average 2.042(6) Å) in the cyclometalating ligands, and the values are similar to those found in the literature for (C∧ N)-cyclometalated complexes.[44,46,49] The Ir−O bond length (2.132(6)−2.139(6) Å) and the Ir−N1 and Ir−N3 bond

dx.doi.org/10.1021/ic200704s |*Inorg. Chem.* 2011, 50, 8197–8206

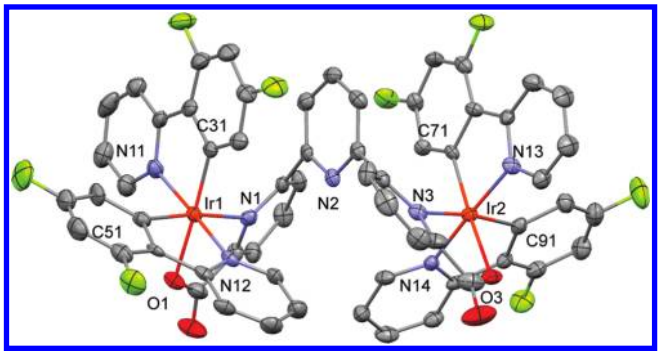

Figure 2. ORTEP drawing of the molecular structure of the iridium complex **Ir2** (thermal ellipsoids at 35% probability level; H atoms omitted for simplicity).

lengths (2.216(7)−2.205(7) Å) are longer than the average values reported in the Cambridge Crystallographic Database,[51] consistent with the large trans influence of the phenyl groups. The mean value of the N12−Ir1−N11 and N14−Ir2−N13 angles is 176.3(6)°, similar to the C31−Ir1−O1 and C71−Ir2−O3 angles (mean value = 175.0(3)°), and reflects the orthogonality of the ligands. Due to steric hindrance, the terminal pyridine unit is tilted, decreasing the C51−Ir1−N1 and C91−Ir2−N3 angles to an average of 172.3(9)°.

The largely distorted terpyridine unit acts as a bridge between the two iridium centers, bringing them at a longer nonbonding intermetallic distance of 7.47 Å compared to 3.77 Å for the chlorine-bridged dimeric complex **2**. Due to the constraints of accommodating the iridium complexes, the terminal pyridine ring planes are twisted (61.9°) compared to the central ring plane. Intramolecular $\pi-\pi$ interactions occur between the central pyridine and the cyclometalating phenyl rings, situated at a distance of 3.22 and 3.24 Å, respectively (Figure S1, Supporting Information).

Solution Structure. The solution ^{1}H NMR spectra (Figure S2, Supporting Information) of the bimetallic iridium complexes **Ir1** and **Ir2** in d_2-tetrachloroethane and d_2-dichloromethane, respectively, display only one set of proton signals (21 resonances for **Ir1** and 17 for **Ir2**), which have been assigned by 2D ^{1}H−^{1}H COSY and NOESY experiments. These features indicate the presence of symmetric solution species with two equivalent iridium centers on the NMR time scale, in agreement with the pseudo-C_2 symmetry observed in the crystal structure of the **Ir2** complex. (In **Ir2** within each iridium coordination sphere, the two phenylpyridine ligands are nonequivalent and arranged in a *trans*-N,N disposition.) This suggests that only the enantiomeric ΔΔ and ΛΛ species are found in solution, in contrast with a recently reported dimeric iridium phenylpyridine complex containing a dipyridyl−phenanthroline bridging ligand which is present in solution as a diastereomeric mixture of ΔΛ, ΔΔ, and ΛΛ species.[37]

Absorption and Emission Spectroscopy. The absorption spectra of **Ir1** and **Ir2** (Figure 3) measured in an air-saturated dichloromethane solution at room temperature were assigned by comparing with similar phenylpyridine-based complexes.[18,20,34,44,45,49] The binuclear compounds show intense bands in the region 250−350 nm which can be attributed to the spin-allowed singlet $^1\pi-\pi^*$ ligand-centered (LC) transitions. This assignment suggests that the LC transitions of the phenylpyridine and bridging ligand fall in the same region, similarly to what was observed for other dinuclear complexes

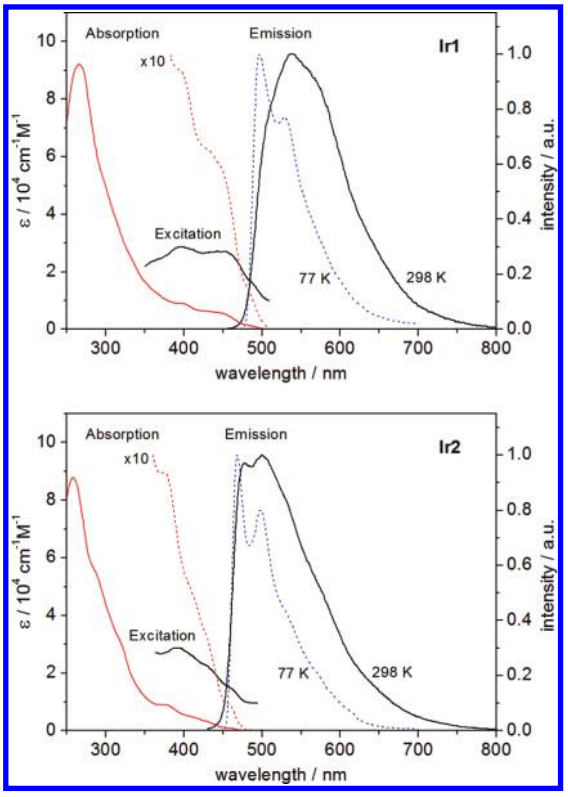

Figure 3. UV−vis absorption spectra and excitation and normalized emission spectra at 298 (solid line) and 7 7K (dotted line) for complexes **Ir1** (top) and **Ir2** (bottom) in 10^{-4} mol·dm^{-3} CH_2Cl_2 solutions.

containing aromatic amines as bridging ligands.[34] The high-energy maximum of **Ir1** at 266 nm ($\varepsilon \approx 9.2 \times 10^4$ M^{-1}·cm^{-1}) is shifted hypsochromically to 258 nm ($\varepsilon \approx 8.8 \times 10^4$ M^{-1}·cm^{-1}) in **Ir2**. Compared to the well-known mononuclear complexes [Ir(ppy)$_2$(pic)] (ppyH = 2-phenylpyridine, picH = picolinic acid)[52] and [Ir(Fppy)$_2$(pic)] commonly referred as FIrpic (FppyH = 2′-(4,6-difluorophenyl)pyridine),[43] the molar extinction coefficient is roughly doubled in the bis-iridium complexes **Ir1** and **Ir2** (Figure S3, Supporting Information). In the lower energy region (>350 nm), the spectra of the complexes exhibit weaker ($\varepsilon \approx 5-9 \times 10^3$ M^{-1}·cm^{-1}) absorption tails, which can be assigned to the dπ(Ir) → π(ligand) metal-to-ligand charge transfer (MLCT) transitions, as reported for similar cyclometalated complexes.[20,53] In the case of **Ir2**, these bands are blue shifted by ∼20 nm compared to the non-fluorinated analogue **Ir1**, with intense transitions at, respectively, 373 and 395 nm, which correspond to singlet ^{1}MLCT states. The formally spin-forbidden triplet dπ(Ir) → π^*(ligand) ^{3}MLCT transitions from the singlet ground state S_0 to the lowest triplet states gain intensity by mixing with the higher lying ^{1}MLCT transitions through the strong spin−orbit coupling of iridium and appear as weak shoulders in the range 400−500 nm in both **Ir1** and **Ir2**. Overall, both dinuclear complexes exhibit very similar absorption features (apart from the increased intensity) compared to the mononuclear references [Ir(ppy)$_2$(pic)] and [Ir(Fppy)$_2$(pic)], suggesting that the bridging ligand makes only a small contribution to the absorption process in these systems.

The emission and excitation spectra of the **Ir1** and **Ir2** complexes in degassed dichloromethane solutions at room (298 K) and low (77 K) temperature are compared in Figure 3. The excitation spectrum reproduces the shape of the

dx.doi.org/10.1021/ic200704s |*Inorg. Chem.* 2011, 50, 8197–8206

Table 3. Summary of Photophysical Properties[a] for Complexes Ir1 and Ir2 Measured in Degassed Dichloromethane Solutions at 298 and 77 K Together with Literature Data for Relevant Monometallic Complexes for Comparison

	emission, 298 K[b]				emission, 77 K[b]		
	λ_{max}/nm	$\tau/\mu s$[c]	$k_r/10^5\ s^{-1}$	$\Phi/\%$[c]	λ_{max}/nm	$\tau/\mu s$[c]	refs
Ir1	538	0.09(1)	19.7	17.7(3)	496	5.81(2)	this work
Ir2	477	0.15(1)	3.2	4.8(1)	468	3.19(2)	this work
$[Ir(ppy)_2pic]$	505	1.4	2.1	29			52
$[Ir(Fppy)_2pic]$	468	1.4	3.0	42			21

[a] Emission wavelengths (λ), excited state lifetimes (τ), radiative rate constants (k_r), and absolute emission quantum yields (Φ). [b] Excitation wavelength 375 nm. [c] Emission wavelength 533 nm.

components of the absorption spectrum recorded at the same concentration, with the ^{1}MLCT and spin-forbidden ^{3}MLCT transitions appearing at 397 and 450 nm for **Ir1** and 477 and 500 nm for **Ir2**, respectively. The emission spectrum of **Ir1** at room temperature is dominated by a broad band centered at 538 nm. The emission of **Ir2** is characterized by a broad band displaying a finer structure with respect to the emission of **Ir1**, with two components at 477 and 500 nm. The presence of fluorine substituents results in a blue shift of the emission with respect to **Ir1**. This is consistent with what was observed before for mononuclear cyclometalated Ir complexes.[43] The emission of **Ir1** and **Ir2** can be assigned to have a prevalent ^{3}MLCT character on the basis of its shape and recorded lifetimes (0.09 and 0.15 μs for **Ir1** and **Ir2**, respectively) and in agreement with previous characterizations of monometallic complexes coordinated by similar ligands.[18,20,54,55] This attribution will be further substantiated in the computational section. A bathochromic shift of ~35 nm is observed for the bimetallic species **Ir1** with respect to the monometallic complex $[Ir(ppy)_2(pic)]$ (λ_{max} = 505 nm), but the shape of the spectrum remains the same.[52] In the case of **Ir2**, a smaller bathochromic shift of ~10 nm is observed with respect to the FIrpic complex (λ_{max} = 468 nm) while broadened spectral features indicate a more prevalent charge-transfer character with only a minor contribution from the ligand-centered states. The observed displacement indicates that formation of the dinuclear complex has a direct influence on the energy of the emitting states.[15,35] Marked blue or red shifts have been previously observed in the emission of dinuclear complexes with respect to mononuclear ones and have been ascribed to ^{3}MLCT transitions involving the bridging ligand.[33,36] This is further confirmed when we compare the $^3\pi\pi^*$ state 0-phonon transitions in the cyclometalating and bridging ligand, measured at 77 K in dichloromethane glass. Since the triplet excited states of the terpyridine−dicarboxylate (434 nm, 2.86 eV) are found at a similar level as those of the phenylpyridine (436 nm, 2.85 eV) and below those of difluorophenylpyridine (412 nm, 3.01 eV) ligands, the lowest MLCT state of the iridium complexes should contain a significant contribution from the terpyridine moiety.

The lifetimes of emission and absolute emission quantum yields determined for complexes **Ir1** and **Ir2** in degassed dichloromethane solutions are given in Table 3. The room temperature emission has a short monoexponential decay which corresponds to lifetimes of 0.09 and 0.15 μs for complexes **Ir1** and **Ir2**, respectively, while the low-temperature emission is much longer (5.81 and 3.19 μs, respectively). The radiative rate constants can be calculated from the room temperature data as $k_r = \Phi\ \tau^{-1}$ and amount to 19.7×10^5 and $3.2 \times 10^5\ s^{-1}$ for the **Ir1** and **Ir2**, respectively. This is in agreement with the ^{3}MLCT nature of the excited states, for which fast rate constants above $2 \times 10^5\ s^{-1}$ are typically found.[15] The quantum yields of the emissions are highly sensitive to oxygen, which also confirms that the emission arises from a triplet state MLCT in nature. The emission quantum yields observed for the two diiridium complexes are sizable, and the value of the emission quantum yield for **Ir1** shows only an 11% decrease with respect to the emission quantum yield reported for the mononuclear analogue $[Ir(ppy)_2pic]$ (29%). Moreover, the emission efficiency measured for **Ir1** is among the highest observed for dinuclear iridium complexes.[15] Notably, most dinuclear complexes show very low emission quantum yields (<1%)[15,33,34,36−40] compared to their mononuclear analogues, and to our knowledge, only two dinuclear complexes with higher emission quantum yields (12% and 18%) have been reported previously.[32,35] The nonfluorinated complex **Ir1** shows a significantly larger value (~18%) compared to the fluorinated analogue **Ir2** (~5%), suggesting an important substituent effect on the emission properties.

Theoretical Outcomes. DFT and TD-DFT calculations were employed to gain insights into the electronic structure of these systems and to provide a deeper characterization of the excited states involved in the absorption and emission processes of **Ir1** and **Ir2**. DFT and TD-DFT studies have been increasingly used in the past few years to assign the excited states involved in the absorption and emission processes, to rationalize the factors determining the efficiency of radiative and nonradiative deactivation pathways in iridium complexes, and to tune the excited state properties in a combined experimental and theoretical approach.[21,22,57−68] We therefore decided to use DFT and TD-DFT calculations to gain insights into the electronic structure of the dinuclear iridium systems presented here and to provide a deeper characterization of the excited states involved in the absorption and emission processes of complexes **Ir1** and **Ir2**.

From a structural point of view, in order to assess the quality of our computational approach, the computed ground-state structure of **Ir2**, fully optimized at the DFT level, was compared with the available X-ray diffraction data. Generally, excellent agreement between the computed (Table S3, Supporting Information) and observed bond lengths and angles is found, especially when considering the Ir(III) first coordination sphere. For example, average computed bond distances for Ir−O, Ir−C, and Ir−N(ppy) of 2.148(0), 1.997(3), and 2.041(1) Å, respectively, compare very well to the corresponding experimental values of 2.136(5), 1.995(8), and 2.042(6) Å, respectively. Bond angles are also accurately reproduced, apart from a few cases (such as C51−Ir1−O1 or C31−Ir1−N1) for which angles differ by ca. 3°. This is probably due to the presence of solvent molecules in the crystal structure near that site, responsible for

dx.doi.org/10.1021/ic200704s |Inorg. Chem. 2011, 50, 8197–8206

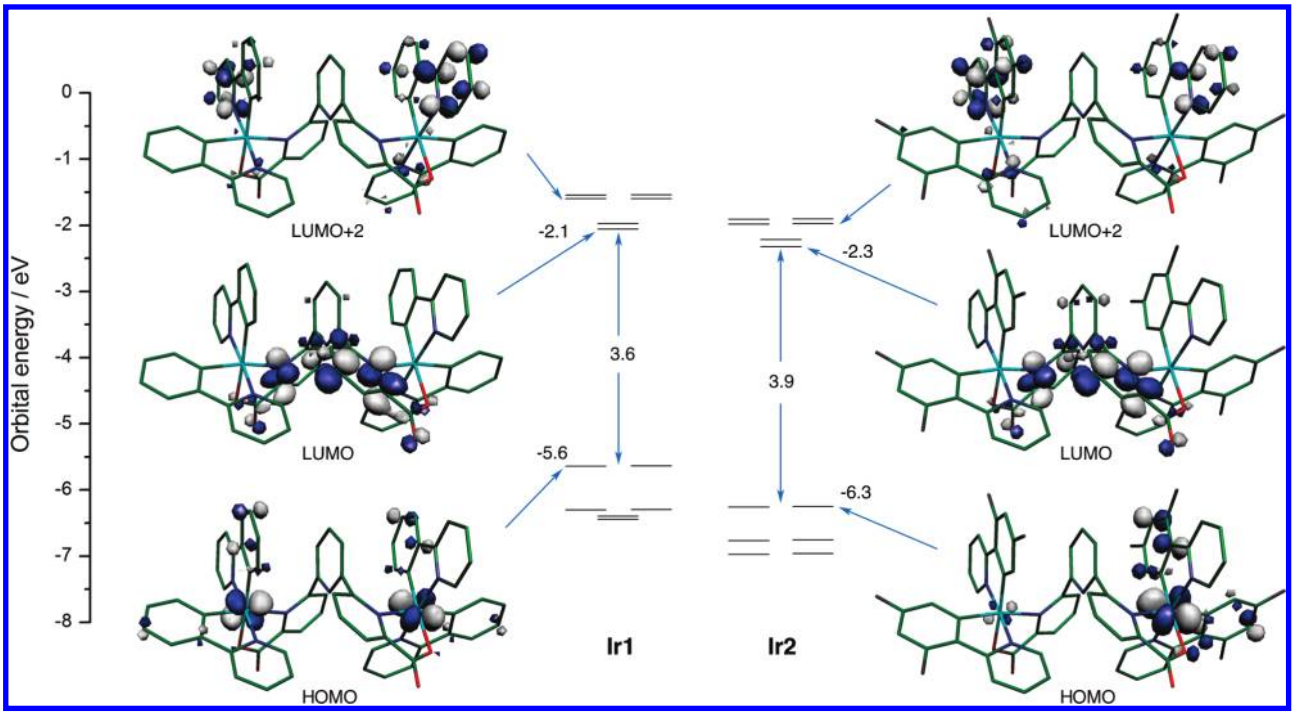

Figure 4. Computed energy levels (in eV) and contour plots (isocontour value of 0.05 au) of selected molecular orbitals of **Ir1** and **Ir2**. For clarity, H atoms have been omitted as well as MOs below the HOMO−5 and above the LUMO+5.

these slight distortions of the structure. Such effects are not expected to be modeled using an implicit solvation model such as CPCM.

In order to analyze the electronic structure of these systems the energy of the six highest occupied and of the six lowest unoccupied molecular orbitals (MO) are reported in Figure 4, together with the contour plots of some most relevant MOs.

The overall orbital picture is fully consistent with that expected for a pseudo-octahedral coordinated Ir(III) system. In particular, the highest occupied molecular orbitals (HOMO and HOMO−1) of both **Ir1** and **Ir2** complexes are a degenerate couple showing a significant contribution from the 5d Ir(t_{2g}) orbitals and a smaller π contribution from the phenyl units of the cyclometalating ppy ligands. Due to the presence of electron-withdrawing groups (fluorine), in the case of **Ir2**, the energy of the HOMO is decreased with roughly 0.6 eV when compared to **Ir1**. The HOMOs are followed, in order of decreasing energy, by two other degenerate orbitals (HOMO−2 and HOMO−3) also displaying a large contribution from 5d orbitals centered on the Ir atoms with smaller percentages from p orbitals of the oxygen atom of the carboxylic acid group of the terpyridine ligand. On the contrary, the lowest unoccupied molecular orbitals (LUMO and LUMO+1) of both complexes are a degenerate couple of MO of π^* character centered on the ancillary terpyridine−dicarboxylate ligand, with no relevant contribution from Ir orbitals. In the case of **Ir2**, the presence of the fluorine groups only weakly influences the stability of the LUMO level (showing no contribution from the phenylpyridine ligands), so that the LUMO of **Ir2** is lying only roughly 0.3 eV lower in energy with respect to the LUMO of **Ir1**. As a consequence, the computed HOMO−LUMO energy gap is slightly larger for the **Ir2** compound (3.58 and 3.93 eV for **Ir1** and **Ir2**, respectively) for

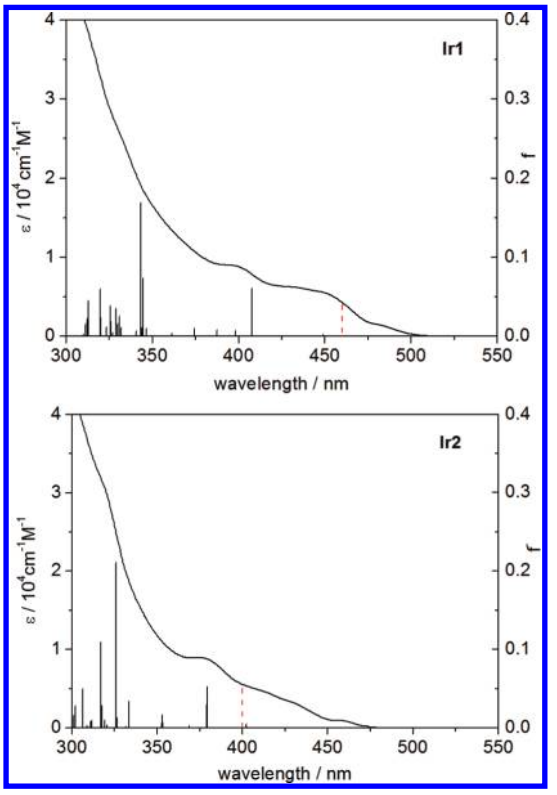

Figure 5. Computed singlet to singlet (vertical black bar) and singlet to triplet (vertical red dashed bar) excitations together with the experimental absorption spectra (black curve) of **Ir1** and **Ir2**.

which a small but sizable blue shift of the first absorption band is thus expected.[22] At higher energies are found two pairs of

dx.doi.org/10.1021/ic200704s |*Inorg. Chem.* 2011, 50, 8197–8206

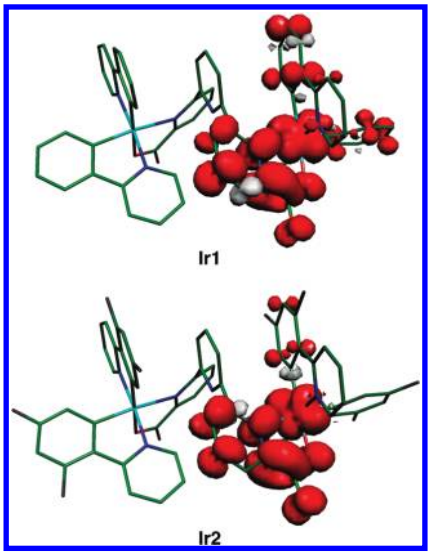

Figure 6. Computed spin densities of the vertical T_1 state for complexes **Ir1** and **Ir2** (isocontour value 0.0025 au; H atoms have been omitted for clarity).

degenerate orbitals (LUMO+2 and LUMO+3; LUMO+4 and LUMO+5) all localized on the cyclometalating phenylpyridine ligands. The energy gap between the LUMO orbital centered on the terpyridine−dicarboxylate ligand and the LUMO+2 orbital centered on phenylpyridine is small (0.4 and 0.3 eV for **Ir1** and **Ir2**, respectively). Overall, the computed orbital picture is consistent with a scenario where the first observed transitions will be of MLCT character, corresponding to excitation from the occupied frontier orbitals (of Ir(t_{2g}) character) to ligand-centered orbitals (of π^* character).

In order to better characterize this low-energy UV−vis spectral region, TD-DFT calculations were performed for both **Ir1** and **Ir2** complexes. In particular, the lowest S_0−S_n vertical excitation energies were computed in order to have access to the spectral region below 325 nm. These transitions are reported as vertical bars in Figure 5 in order to easily compare with the available experimental data (full raw data available as Tables S4 and S5, Supporting Information). In this spectral region, all computed transitions have a dominant MLCT character but those occurring at higher energy, close to 325 nm, start to display mixed MLCT/LC contributions. This spectral region presents two dominant transitions computed at 408 and 343 nm and at 379 and 326 nm for **Ir1** and **Ir2**, respectively. Few other transitions of lower intensity are also computed in the same region, and most probably they contribute to yield the complex broad band structure experimentally detected. The main computed transitions compare well with the maxima of absorption experimentally defined at 395 and 330 nm and at 373 and 320 nm for **Ir1** and **Ir2**, respectively. In particular, the blue shift of these bands going from **Ir1** to **Ir2**, also expected by simple inspection of the HOMO−LUMO gap for the two compounds, is qualitatively and quantitatively reproduced by calculations.

Nevertheless, the low-energy experimental band (at 445 and 425 nm for **Ir1** and **Ir2**, respectively) is clearly missing in the computed transitions. Since this band is most probably due to a spin-forbidden singlet to triplet excitation, the energy of the first vertical triplet state was also estimated for both compounds using a ΔSCF approach. As in the case of singlet excited state, the first triplet vertical transition is computed to be significantly blue shifted when going from **Ir1** (460 nm) to **Ir2** (400 nm) and nicely compare with the first observed energy band for the first compound while it seems overestimated for the latter.

In conclusion, from our calculations it seems clear that the low-energy spectral region is dominated by MLCT transitions, the lowest edge of the spectra being ascribable to a ^{3}MLCT transition. Interestingly, analysis of the spin density maps (Figure 6) computed for the two systems allows one to clearly highlight that while in the case of **Ir1** the LC contributions to the ^{3}MLCT are located on both the picolinate unit of the bridging terpyridine (major) as well as on the phenylpyridine ligand (minor), in the case of **Ir2** the ligand contribution is mainly arising from the picolinate unit of the bridging ligand. This should play an important role in the observed differences in emission quantum yields for the two complexes.

Thus, the first triplet states responsible for the emissive properties in both systems were fully optimized in order to allow for a fair comparison with luminescence data. Comparison of calculated emission maxima, 530 and 470 nm for **Ir1** and **Ir2**, respectively, shows a good agreement with the values determined by the experimental measurements at 77 K (496 and 468 nm, respectively) and 298 K (538 and 477 nm, respectively). The used ΔSCF method successfully predicts these transitions and assigns them as a mixing of ^{3}MLCT and ^{3}LC levels.

The good agreement between the computed and the experimental spectra obtained even for such complex systems containing two coupled Ir centers allows the use of DFT-based methods to be envisaged for prediction and design of new molecular species possessing selected absorption or emission features.

CONCLUSIONS

We reported here on the preparation, structural and photophysical characterization, as well as theoretical investigation of a new class of homopolymetallic architectures containing covalently linked bis-iridium complexes bridged by a terpyridine−carboxylate unit. The facile synthetic protocol, together with the good photophysical properties of the resulting complexes (emission quantum yields up to 18%), suggests that such architectures are of potential interest for the development of polymetallic assemblies with optimized optical properties. Moreover, the bridging ligand has a direct influence on the energy of the emitting states, leading to a red shift with respect to analogous monometallic complexes. The easy access to substituted terpyridine−carboxylate ligands anticipates the possibility of tuning the emission wavelength and optimizing the emission quantum yield of these dinuclear iridium complexes. Work in this direction is in progress. Future studies will also be directed to develop higher nuclearity complexes with related ligands. DFT studies reproduce well the experimental data and show an important effect of the nature of both peripheral and bridging ligands on the emissive properties of the two diiridium complexes. This suggest that the effects of chemical functionalization on the bridging and cyclometalating ligands could be easily screened by TD-DFT methods, allowing one to propose new systems with improved optical properties.

EXPERIMENTAL SECTION

General Methods, Equipment, and Chemicals Used. Solvents and starting materials were purchased from Aldrich, Fluka, or Acros and used without further purification, unless otherwise stated. ^{1}H and ^{13}C NMR spectra were recorded at 298 K for characterization purposes on Bruker Advance 200 and Varian Unity 400 spectrometers. Chemical shifts are reported in ppm and were referenced internally to the residual solvent resonance. Mass spectra were run on a Thermo Scientific LXQ mass spectrometer equipped with an electrospray source. Elemental analyses were performed by the Service Central d'Analyses of CNRS (Vernaison, France). Bis-μ-chloride-bridged diiridium complexes **1**[17,45] and **2**[17] as well as 2-(2,4-difluorophenyl)pyridine[17] and terpyridine dicarboxylate acid[69] were prepared according to literature procedures.

X-ray Crystallography. Diffraction data were collected using a Bruker SMART CCD area detector three-circle diffractometer (Mo Kα radiation, graphite monochromator, λ = 0.71073 Å), controlled by the Bruker SMART software.[70] To prevent evaporation of cocrystallized solvent molecules, the crystals were coated with a light hydrocarbon oil. At the end of data collection, the first 50 frames were recollected to verify that crystal decay had not taken place during the experiment. Unique intensities with $I > 10\sigma(I)$ detected on all frames using the Bruker SAINT program[71] were used to refine the values of the cell parameters. The substantial redundancy in data allows empirical absorption corrections to be applied using multiple measurements of equivalent reflections with the Bruker SADABS programs.[72] Space groups were determined from systematic absences, and they were confirmed by the successful resolution of the structures. The structures were solved by direct methods using the Bruker SHELXTL 6.14 package,[73] and all atoms, including hydrogen atoms, were found by difference Fourier syntheses. All non-hydrogen atoms were anisotropically refined on F, whereas hydrogen atoms were refined isotropically. Experimental details for X-ray data collections are given in Table 2.

Photophysical Measurements. Absorption spectra were recorded in 1 cm quartz cells on a Cary 50 Probe UV−vis spectrophotometer. Low-resolution visible luminescence measurements in solution were recorded on a Perkin-Elmer LS-50B spectrometer at 298 K. For spectral measurements at low temperature, the spectrometer was fitted with a solid state adaptor equipped with a liquid nitrogen cooling system. Quartz cells with an optical path of 1 cm were used for room temperature spectra, while 77 K measurements were carried out in quartz capillaries 3 mm in diameter. The general layout of the instrumental setup for the lifetime measurements was as follows. A tunable Coherent CR-599 dye laser (band path 0.03 nm, 50−300 mW) was pumped by a continuous Coherent Innova-90 argon laser (8 W) for which the lines at 465.8, 488, and 514 nm were used for excitation. The emitted light was analyzed at 90° with a Spex 1870 single monochromator with 950 g/mm holographic gratings blazed at 900 nm. The output signal of the photomultiplier was fed into a Lecroy LT262 oscilloscope (1 GHz) to avoid saturation of the signal and then into a Standford Research SR-430 multichannel scaler. Data were transferred into a PC and corrected for the instrumental function. Low-temperature measurements were performed with the help of a CTI-Cryogenics Cryodyne M-22 closed-cycle refrigerator controlled by a Lakeshore 321 temperature controller. Phosphorescence lifetime and emission quantum yield measurements were done on a Fluorolog FL 3-22 spectrometer from Spex-Jobin-Yvon-Horiba equipped with double grating emission and excitation monochromators and a R928P photomultiplier. The phosphorescence lifetimes were measured by recording the decay at the maximum of the emission spectra. The signals were analyzed as monoexponential decays in the OriginLab OriginPro 8 software, and the values reported are the average of three independent determinations. Absolute emission quantum yields in solution were determined using the Fluorolog FL 3-22 fitted with a home-modified integrating sphere from Oriel, and the procedure is described elsewhere.[74] Emission quantum yields were checked against a reference sample of [Ir(ppy)$_3$] with an emission QY = 40%. Emission and excitation spectra were corrected for source intensity and emission spectral response.

Synthesis of Tetrakis(2-phenylpyridine)μ-(2,2′:6′,2″-terpyridine-6,6″-dicarboxylic acid)diiridium Complex (Ir1). Terpyridine dicarboxylate acid (14.9 mg, 0.046 mmol) was suspended in methanol (10 mL) and reacted with a 1 N KOH solution in methanol (92 μL, 0.092 mmol) to give **3**. The solvent was evaporated under vacuum, and the resulting salt was suspended in ethoxyethanol (5 mL) under argon. The [tetrakis(2-phenylpyridine)-(μ-dichloro)diiridium precursor **1** (49.6 mg, 0.046 mmol) was added, and the mixture was stirred under argon at 60 °C for 20 h. The resulting precipitate was filtered, washed with chloroform, and recrystallized from dichloromethane−chloroform to afford 52.4 mg (86%) of a yellow product. ^{1}H NMR (200 MHz, $C_2D_2Cl_4$): δ ppm 8.68 (d, J = 4.3 Hz, 2H), 8.40 (d, J = 4.3 Hz, 2H), 8.34 (d, J = 7.4 Hz, 2H), 7.75 (t, J = 7.3 Hz, 2H), 7.68−7.60 (m, 8H), 7.48−7.45 (m, 4H), 7.17 (d, J = 7.2 Hz, 2H), 7.07 (d, J = 7.1 Hz, 2H), 6.98 (dd, J = 5.7, 4.9 Hz, 2H), 6.81 (t, J = 6.8 Hz, 2H), 6.61 (t, J = 6.7 Hz, 2H), 6.41 (t, J = 6.6 Hz, 2H), 6.30 (tbr, 1H), 6.24 (tbr, 2H), 6.07 (t, J = 6.9 Hz, 2H), 5.71 (d, J = 7.3 Hz, 2H), 5.35 (d, J = 6.5 Hz, 2H). ES$^+$-MS m/z: 1319.9 [**Ir1**]H$^+$. Anal. Calcd for $C_{61}H_{41}Ir_2N_7O_4 \cdot 1.5CHCl_3$: C, 50.06; H, 2.86; N, 6.54. Found: C, 49.95; H, 2.89; N, 6.78.

Synthesis of Tetrakis(2-(2,4-difluorophenyl)pyridine))μ-(2,2′:6′,2″-terpyridine-6,6″-dicarboxylic acid)diiridium Complex (Ir2). Terpyridine dicarboxylate acid (17.3 mg, 0.054 mmol) was suspended in methanol (10 mL) and reacted with a 1 N KOH solution in methanol (108 μL, 0.108 mmol) to give **3**. The solvent was evaporated under vacuum, and the resulting salt was suspended in ethoxyethanol (5 mL) under argon. The [tetrakis(2-(2,4-difluorophenyl)pyridine)-(μ-dichloro)diiridium precursor **2** (65.7 mg, 0.054 mmol) was added, and the mixture was stirred under argon at 60 °C for 20 h. The resulting suspension was filtered; then the filtrate was evaporated and separated by column chromatography on alumina using chloroform and chloroform−ethylacetate−ethanol (20:5:1). The product was finally obtained after recrystallization from dichloromethane−chloroform as 19.4 mg (25%) of a yellow powder. ^{1}H NMR (200 MHz, CD_2Cl_2): δ ppm 8.95 (dd, J = 5.7, 0.9 Hz, 2H), 8.46 (dd, J = 7.7, 1.3 Hz, 2H), 8.42 (dbr, 2H), 8.13 (d, J = 8.2 Hz, 4H), 7.85 (t, J = 7.7 Hz, 2H), 7.76 (t, J = 7.8 Hz, 2H), 7.59 (t, J = 7.7 Hz, 2H), 7.27 (td, J = 7.6, 1.2 Hz, 2H), 7.15 (ddd, J = 7.2, 5.9, 1.3 Hz, 2H), 6.85 (t, J = 7.7 Hz, 1H), 6.38 (d, J = 7.7 Hz, 2H), 6.36 (ddd, J = 12.2, 9.6, 2.3 Hz, 2H), 6.25 (ddd, J = 7.2, 5.9, 1.2 Hz, 2H), 6.11 (ddd, J = 12.2, 9.6, 2.3 Hz, 2H), 5.24 (dd, J = 8.7, 2.3 Hz, 2H), 4.81 (dd, J = 8.3, 2.3 Hz, 2H). ES$^+$-MS m/z: 1465.8 [**Ir2**]H$^+$. Anal. Calcd for $C_{61}H_{33}F_8Ir_2N_7O_4 \cdot 0.6CHCl_3$: C, 48.17; H, 2.20; N, 6.38. Found: C, 48.19; H, 2.47; N, 6.55.

Computational Methods. Ground-state structures of **Ir1** and **Ir2** complexes were fully optimized at the DFT level using the PBE0 exchange correlation functional[75]combined with a double-ξ quality basis (LANL2DZ)[76] and corresponding pseudopotential[77] for the Ir(III) atoms using the Gaussian package.[78] The hybrid PBE0 exchange-correlation functional mixes exact (Hartree−Fock) and PBE exchange in a 1:3 ratio. Previous studies at such level of theory have demonstrated that this approach is able to accurately model the structural and spectroscopic properties of a wide variety of organometallic systems.[79,80] For both systems, subsequent frequency calculations were performed in order to confirm the nature of the stationary point found (minimum). TD-DFT[81] and ΔSCF[82] approaches were employed to gain insights into the absorption and emission processes, respectively. In particular, the 20 lowest singlet−singlet excitations were analyzed in order to compute and assign the absorption spectra. In the following only vertical transitions with non-negligible intensity will be discussed.

In order to characterize the triplet emissive state, a full structural optimization of the triplet state for both system was performed at the unrestricted level of theory. For both ground and excited state calculations, solvent effects were taken into account via the conductor-like polarizable continuum model (CPCM) considering dichloromethane as solvent.

■ ASSOCIATED CONTENT

Supporting Information. X-ray crystallographic data for compounds **2** and **Ir2** in CIF format; crystal packing structure of **Ir2**; ^{1}H NMR spectra and complete proton assignment for **Ir1** and **Ir2**; absorption and emission spectra compared between FIrpic and **Ir2**; computed Cartesian coordinates for **Ir1** and **Ir2**; compared bond distances and angles for **Ir2**; lowest vertical excitation energies for **Ir1** and **Ir2**. This material is available free of charge via the Internet at http://pubs.acs.org.

■ AUTHOR INFORMATION

Corresponding Author

*E-mail: marinella.mazzanti@cea.fr (M.M.); adrian.calborean@itim-cj.ro (A.C.).

■ ACKNOWLEDGMENT

E.S.A. was supported by the European Community under the FP6Marie Curie Host Fellowships for EST "CHEMTRONICS" MEST-CT-2005-020513. We thank Pierre-Alain Bayle for his help with the NMR measurements, Colette Lebrun for recording mass spectra, and Jean-Claude Bünzli for providing access to spectroscopy equipment.

■ REFERENCES

(1) Lowry, M. S.; Bernhard, S. *Chem.—Eur. J.* **2006**, *12*, 7970–7977.
(2) Chou, P. T.; Chi, Y. *Chem.—Eur. J.* **2007**, *13*, 380–395.
(3) Evans, R. C.; Douglas, P.; Winscom, C. J. *Coord. Chem. Rev.* **2006**, *250*, 2093–2126.
(4) Holder, E.; Langeveld, B. M. W.; Schubert, U. S. *Adv. Mater.* **2005**, *17*, 1109–1121.
(5) Sun, Y. R.; Giebink, N. C.; Kanno, H.; Ma, B. W.; Thompson, M. E.; Forrest, S. R. *Nature* **2006**, *440*, 908–912.
(6) Baldo, M. A.; Thompson, M. E.; Forrest, S. R. *Nature* **2000**, *403*, 750–753.
(7) You, Y.; Park, S. Y. *Dalton Trans.* **2009**, 1267–1282.
(8) Lo, K. K. W.; Louie, M. W.; Zhang, K. Y. *Coord. Chem. Rev.* **2010**, *254*, 2603–2622.
(9) Natrajan, L. S.; Toulmin, A.; Chew, A.; Magennis, S. W. *Dalton Trans* **2010**, *39*, 10837–10846.
(10) Zhao, Q.; Yu, M. X.; Shi, L. X.; Liu, S. J.; Li, C. Y.; Shi, M.; Zhou, Z. G.; Huang, C. H.; Li, F. Y. *Organometallics* **2010**, *29*, 1085–1091.
(11) Jiang, W. L.; Gao, Y.; Sun, Y.; Ding, F.; Xu, Y.; Bian, Z. Q.; Li, F. Y.; Bian, J.; Huang, C. H. *Inorg. Chem.* **2010**, *49*, 3252–3260.
(12) Murphy, L.; Congreve, A.; Palsson, L. O.; Williams, J. A. G. *Chem. Commun.* **2010**, *46*, 8743–8745.
(13) Yu, M. X.; Zhao, Q.; Shi, L. X.; Li, F. Y.; Zhou, Z. G.; Yang, H.; Yia, T.; Huang, C. H. *Chem. Commun.* **2008**, 2115–2117.
(14) Lo, K. K. W.; Zhang, K. Y.; Leung, S. K.; Tang, M. C. *Angew. Chem., Int. Ed.* **2008**, *47*, 2213–2216.
(15) Flamigni, L.; Barbieri, A.; Sabatini, C.; Ventura, B.; Barigelletti, F. *Top. Curr. Chem.* **2007**, *281*, 143–203. During the reviewing process a tetranuclear iridium complex has been reported which shows high luminescence quantum yield: Baranoff, E.; Orselli, E.; Allouche, L.; Di Censo, D.; Scopelliti, R.; Grätzel, M.; Nazeeruddin, M. K. *Chem. Commun.* **2011**, *47*, 2799–2801.
(16) Endo, A.; Suzuki, K.; Yoshihara, T.; Tobita, S.; Yahiro, M.; Adachi, C. *Chem. Phys. Lett.* **2008**, *460*, 155–157.
(17) Coppo, P.; Plummer, E. A.; De Cola, L. *Chem. Commun.* **2004**, 1774–1775.
(18) Tamayo, A. B.; Alleyne, B. D.; Djurovich, P. I.; Lamansky, S.; Tsyba, I.; Ho, N. N.; Bau, R.; Thompson, M. E. *J. Am. Chem. Soc.* **2003**, *125*, 7377–7387.
(19) Stagni, S.; Colella, S.; Palazzi, A.; Valenti, G.; Zacchini, S.; Paolucci, F.; Marcaccio, M.; Albuquerque, R. O.; De Cola, L. *Inorg. Chem.* **2008**, *47*, 10509–10521.
(20) Lamansky, S.; Djurovich, P.; Murphy, D.; Abdel-Razzaq, F.; Lee, H. E.; Adachi, C.; Burrows, P. E.; Forrest, S. R.; Thompson, M. E. *J. Am. Chem. Soc.* **2001**, *123*, 4304–4312.
(21) You, Y. M.; Park, S. Y. *J. Am. Chem. Soc.* **2005**, *127*, 12438–12439.
(22) Avilov, I.; Minoofar, P.; Cornil, J.; De Cola, L. *J. Am. Chem. Soc.* **2007**, *129*, 8247–8258.
(23) Orselli, E.; Kottas, G. S.; Konradsson, A. E.; Coppo, P.; Frohlich, R.; Frtshlich, R.; De Cola, L.; van Dijken, A.; Buchel, M.; Borner, H. *Inorg. Chem.* **2007**, *46*, 11082–11093.
(24) Tao, Y. T.; Wang, Q.; Yang, C. L.; Wang, Q.; Zhang, Z. Q.; Zou, T. T.; Qin, J. G.; Ma, D. G. *Angew. Chem., Int. Ed.* **2008**, *47*, 8104–8107.
(25) Baranoff, E.; Bolink, H. J.; De Angelis, F.; Fantacci, S.; Di Censo, D.; Djellab, K.; Gratzel, M.; Nazeeruddin, M. K. *Dalton Trans.* **2010**, *39*, 8914–8918.
(26) Balzani, V.; Bergamini, G.; Campagna, S.; Puntoriero, F. *Top. Curr. Chem.* **2007**, 280, 1−36.
(27) Baranoff, E.; Yum, J. H.; Graetzel, M.; Nazeeruddin, M. K. *J. Organomet. Chem.* **2009**, *694*, 2661–2670.
(28) Costa, R. D.; Fernandez, G.; Sanchez, L.; Martin, N.; Orti, E.; Bolink, H. J. *Chem.—Eur. J.* **2010**, *16*, 9855–9863.
(29) Williams, J. A. G. *Chem. Soc. Rev.* **2009**, *38*, 1783–1801.
(30) Flamigni, L.; Barigelletti, F.; Armaroli, N.; Collin, J. P.; Dixon, I. M.; Sauvage, J. P.; Williams, J. A. G. *Coord. Chem. Rev.* **1999**, *192*, 671–682.
(31) Barcina, J. O.; Herrero-Garcia, N.; Cucinotta, F.; De Cola, L.; Contreras-Carballada, P.; Williams, R. M.; Guerrero-Martinez, A. *Chem.—Eur. J.* **2010**, *16*, 6033–6040.
(32) Plummer, E. A.; Hofstraat, J. W.; De Cola, L. *Dalton Trans.* **2003**, 2080–2084.
(33) Vandiemen, J. H.; Hage, R.; Haasnoot, J. G.; Lempers, H. E. B.; Reedijk, J.; Vos, J. G.; Decola, L.; Barigelletti, F.; Balzani, V. *Inorg. Chem.* **1992**, *31*, 3518–3522.
(34) Neve, F.; Crispini, A.; Serroni, S.; Loiseau, F.; Campagna, S. *Inorg. Chem.* **2001**, *40*, 1093–1101.
(35) Lafolet, F.; Welter, S.; Popovic, Z.; De Cola, L. *J. Mater. Chem.* **2005**, *15*, 2820–2828.
(36) Tsuboyama, A.; Takiguchi, T.; Okada, S.; Osawa, M.; Hoshino, M.; Ueno, K. *Dalton Trans.* **2004**, 1115–1116.
(37) Auffrant, A.; Barbieri, A.; Barigelletti, F.; Lacour, J.; Mobian, P.; Collin, J. P.; Sauvage, J. P.; Ventura, B. *Inorg. Chem.* **2007**, *46*, 6911–6919. Auffrant, A.; Barbieri, A.; Barigelletti, F.; Collin, J. P.; Flamigni, L.; Sabatini, C.; Sauvage, J. P. *Inorg. Chem.* **2006**, *45*, 10990–10997.
(38) Whittle, V. L.; Williams, J. A. G. *Dalton Trans.* **2009**, 3929–3940.
(39) Whittle, V. L.; Williams, J. A. G. *Inorg. Chem.* **2008**, *47*, 6596–6607.
(40) Arm, K. J.; Williams, J. A. G. *Dalton Trans.* **2006**, 2172–2174.
(41) Coppo, P.; Duati, M.; Kozhevnikov, V. N.; Hofstraat, J. W.; De Cola, L. *Angew. Chem., Int. Ed.* **2005**, *44*, 1806–1810.
(42) Andreiadis, E. S.; Demadrille, R.; Imbert, D.; Pecaut, J.; Mazzanti, M. *Chem.—Eur. J.* **2009**, *15*, 9458–9476.
(43) Adachi, C.; Kwong, R. C.; Djurovich, P.; Adamovich, V.; Baldo, M. A.; Thompson, M. E.; Forrest, S. R. *Appl. Phys. Lett.* **2001**, *79*, 2082–2084.
(44) Lamansky, S.; Djurovich, P.; Murphy, D.; Abdel-Razzaq, F.; Kwong, R.; Tsyba, I.; Bortz, M.; Mui, B.; Bau, R.; Thompson, M. E. *Inorg. Chem.* **2001**, *40*, 1704–1711.

(45) Nonoyama, M. *Bull. Chem. Soc. Jpn.* **1974**, *47*, 767–768.
(46) Garces, F. O.; Dedeian, K.; Keder, N. L.; Watts, R. J. *Acta Crystallogr., Sect. C: Cryst. Struct. Commun.* **1993**, *49*, 1117–1120.
(47) Neve, F.; Crispini, A.; Campagna, S.; Serroni, S. *Inorg. Chem.* **1999**, *38*, 2250–2258.
(48) Bettington, S.; Tavasli, M.; Bryce, M. R.; Batsanov, A. S.; Thompson, A. L.; Al Attar, H. A.; Dias, F. B.; Monkman, A. P. *J. Mater. Chem.* **2006**, *16*, 1046–1052.
(49) Sprouse, S.; King, K. A.; Spellane, P. J.; Watts, R. J. *J. Am. Chem. Soc.* **1984**, *106*, 6647–6653.
(50) Ragni, R.; Orselli, E.; Kottas, G. S.; Omar, O. H.; Badudri, F.; Pedone, A.; Naso, F.; Farinola, G. M.; De Cola, L. *Chem.—Eur. J.* **2009**, *15*, 136–148.
(51) Fletcher, D. A.; McMeeking, R. F.; Parkin, D. *J. Chem. Inf. Comput. Sci.* **1996**, *36*, 746–749.
(52) Beyer, B.; Ulbricht, C.; Escudero, D.; Friebe, C.; Winter, A.; Gonzalez, L.; Schubert, U. S. *Organometallics* **2009**, *28*, 5478–5488.
(53) Colombo, M. G.; Brunold, T. C.; Riedener, T.; Gudel, H. U.; Fortsch, M.; Burgi, H. B. *Inorg. Chem.* **1994**, *33*, 545–550.
(54) Laskar, I. R.; Hsu, S. F.; Chen, T. M. *Polyhedron* **2006**, *25*, 1167–1176.
(55) Rausch, A. F.; Thompson, M. E.; Yersin, H. *Inorg. Chem.* **2009**, *48*, 1928–1937.
(56) Colombo, M. G.; Gudel, H. U. *Inorg. Chem.* **1993**, *32*, 3081–3087.
(57) Hay, P. J. *J. Phys. Chem. A* **2002**, *106*, 1634–1641.
(58) Ladouceur, S.; Fortin, D.; Zysman-Colman, E. *Inorg. Chem.* **2010**, *49*, 5625–5641.
(59) Shi, L. L.; Geng, Y.; Gao, H. Z.; Su, Z. M.; Wu, Z. J. *Dalton Trans.* **2010**, *39*, 7733–7740.
(60) Minaev, B.; Minaeva, V.; Agren, H. *J. Phys. Chem. A* **2009**, *113*, 726–735.
(61) Minaev, B.; Agren, H.; De Angelis, F. *Chem. Phys.* **2009**, *358*, 245–257.
(62) Gu, X.; Fei, T.; Zhang, H. Y.; Xu, H.; Yang, B.; Ma, Y. G.; Liu, X. D. *Eur. J. Inorg. Chem.* **2009**, 2407–2414.
(63) Gu, X.; Fei, T.; Zhang, H. Y.; Xu, H.; Yang, B.; Ma, Y. G.; Liu, X. D. *J. Phys. Chem. A* **2008**, *112*, 8387–8393.
(64) De Angelis, F.; Fantacci, S.; Evans, N.; Klein, C.; Zakeeruddin, S. M.; Moser, J. E.; Kalyanasundaram, K.; Bolink, H. J.; Grätzel, M.; Nazeeruddin, M. K. *Inorg. Chem.* **2007**, *46*, 5989–6001.
(65) Jansson, E.; Minaev, B.; Schrader, S.; Agren, H. *Chem. Phys.* **2007**, *333*, 157–167.
(66) Liu, T.; Zhang, H. X.; Shu, X.; Xia, B. H. *Dalton Trans* **2007**, 1922–1928.
(67) Su, W. L.; Yu, Y. C.; Tseng, M. C.; Wang, S. P.; Huang, W. L. *Dalton Trans.* **2007**, 3440–3449.
(68) Tao, L.; Hong-Xing, Z.; Bao-Hui, X. *J. Phys. Chem. A* **2007**, 8724–8730.
(69) Galaup, C.; Couchet, J. M.; Bedel, S.; Tisnès, P.; Picard, C. *J. Org. Chem.* **2005**, *70*, 2274–2284.
(70) *SMART v. 5.628, Bruker Molecular Analysis Research Tool*; Bruker AXS: Madison, WI, 2002.
(71) *SAINT v. 6.22, Bruker Molecular Analysis Research Tool*; Bruker AXS: Madison, WI, 2002.
(72) *SADABS v. 2.01, An Empirical Absorption Correction Program*; Bruker AXS: Madison, WI, 1995.
(73) *SHELXTL v. 6.14, Structure Determination Software Suite*; Bruker AXS: Madison, WI, 2006.
(74) deMello, J. C.; Wittmann, H. F.; Friend, R. H. *Adv. Mater.* **1997**, *9*, 230–232.
(75) Liu, T.; Xia, B. H.; Zheng, Q. C.; Zhou, X.; Pan, Q. J.; Zhang, H. X. *J. Comput. Chem.* **2010**, *31*, 628–638.
(76) Ciofini, I.; Daul, C. A.; Adamo, C. *J. Phys. Chem. A* **2003**, *107*, 11182–11190.
(77) Hay, P. J.; Wadt, W. R. *J. Chem. Phys.* **1985**, *82*, 299–310.
(78) Frisch, M. J. T., G. W.; Schlegel, H. B.; Scuseria, G. E.; Robb, M. A.; Cheeseman, J. R.; Scalmani, G.; Barone, V.; Mennucci, B.; Petersson, G. A.; Nakatsuji, H.; Caricato, M.; Li, X.; Hratchian, H. P.; Izmaylov, A. F.; Bloino, J.; Zheng, G.; Sonnenberg, J. L.; Hada, M.; Ehara, M.; Toyota, K.; Fukuda, R.; Hasegawa, J.; Ishida, M.; Nakajima, T.; Honda, Y.; Kitao, O.; Nakai, H.; Vreven, T.; Montgomery, Jr., J. A.; Peralta, J. E.; Ogliaro, F.; Bearpark, M.; Heyd, J. J.; Brothers, E.; Kudin, K. N.; Staroverov, V. N.; Kobayashi, R.; Normand, J.; Raghavachari, K.; Rendell, A.; Burant, J. C.; Iyengar, S. S.; Tomasi, J.; Cossi, M.; Rega, N.; Millam, N. J.; Klene, M.; Knox, J. E.; Cross, J. B.; Bakken, V.; Adamo, C.; Jaramillo, J.; Gomperts, R.; Stratmann, R. E.; Yazyev, O.; Austin, A. J.; Cammi, R.; Pomelli, C.; Ochterski, J. W.; Martin, R. L.; Morokuma, K.; Zakrzewski, V. G.; Voth, G. A.; Salvador, P.; Dannenberg, J. J.; Dapprich, S.; Daniels, A. D.; Farkas, Ö.; Foresman, J. B.; Ortiz, J. V.; Cioslowski, J.; Fox, D. J. *Gaussian 09*, Revision A.1; Gaussian, Inc.: Wallingford, CT, 2009.
(79) Boulet, P.; Chermette, H.; Weber, J. *Inorg. Chem.* **2001**, *40*, 7032–7039.
(80) Ciofini, I.; Hazebroucq, S.; Joubert, L.; Adamo, C. *Theor. Chem. Acc.* **2004**, *111*, 188–195.
(81) Stratmann, R. E.; Scuseria, G. E.; Frisch, M. J. *J. Chem. Phys.* **1998**, *109*, 8218–8224.
(82) Guillemoles, J.-F.; Barone, V.; Joubert, L.; Adamo, C. *J. Phys. Chem. A* **2002**, *106*, 11354–11360.